

Article

Effect of C3-Alcohol Impurities on Alumina-Catalyzed Bioethanol Dehydration to Ethylene: Experimental Study and Reactor Modeling

Elena V. Ovchinnikova *, Sardana P. Banzaraktsaeva, Maria A. Kovgan and Victor A. Chumachenko

Boreskov Institute of Catalysis SB-RAS, 5, Lavrentiev Ave., Novosibirsk 630090, Russia

* Correspondence: evo@catalyst.ru; Tel.: +7-383-3269412

Abstract: The impact of feedstock impurities on catalytic process is among the crucial issues for processing real raw materials. A real and model 92%-bioethanol contaminated with 0.03–0.3% mol 1-propanol or 2-propanol were used to make ethylene on a proprietary alumina catalyst in isothermal flow reactor. We proposed a formal kinetic model to describe the impure bioethanol conversion to ethylene and byproducts and used it to evaluate the multi-tubular reactor (*MTR*) for 60 KTPA ethylene production. The simulated data agree well with experimental results. Under reaction-controlled conditions, C3-alcohols strongly suppress the formation of by-products and ethylene-from-ethanol, and slightly inhibit the formation of ethylene-via-ether. It is the suppression of the ethylene-via-ether route that causes a decrease in ethanol conversion. The predominant formation of ethylene-via-ether results in an increased ethylene yield but doubling the catalyst load is required to achieve conversion as for pure feedstock. 2-Propanol has a stronger effect on dehydration than 1-propanol. Diffusion inside the grain's levels out the effect of C3-alcohols on the process in *MTR*, giving an ethylene yield as high as ~98% while dehydrating a contaminated 92% ethanol. However, impurities dilute ethanol and generate propylene (which contaminates target product), and these worsen feedstock consumption and ethylene productivity in *MTR*.

Keywords: bioethanol to ethylene dehydration; alumina catalyst; propanol impurities; kinetic model; mathematical simulation; multi-tubular fixed-bed reactor



Citation: Ovchinnikova, E.V.; Banzaraktsaeva, S.P.; Kovgan, M.A.; Chumachenko, V.A. Effect of C3-Alcohol Impurities on Alumina-Catalyzed Bioethanol Dehydration to Ethylene: Experimental Study and Reactor Modeling. *Catalysts* **2023**, *13*, 509. <https://doi.org/10.3390/catal13030509>

Academic Editors: Maria Jaworska and Piotr Lodowski

Received: 20 January 2023

Revised: 17 February 2023

Accepted: 23 February 2023

Published: 1 March 2023



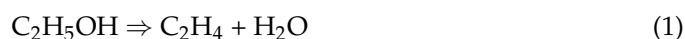
Copyright: © 2023 by the authors. Licensee MDPI, Basel, Switzerland. This article is an open access article distributed under the terms and conditions of the Creative Commons Attribution (CC BY) license (<https://creativecommons.org/licenses/by/4.0/>).

1. Introduction

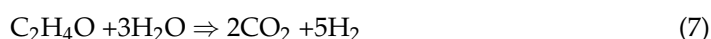
Bioethanol produced from a non-food phytogetic feedstock can be used to manufacture ethylene as a platform product for a great number of downstream derivatives [1–3]. More specifically, polyethylene [1–4], carbon nanotubes [5–7], multi-walled carbon nanotubes [8,9], ethylene oxide [10], and others can be obtained from bioethylene. The impact of impurities on the catalytic process is one of the crucial issues in catalytic technologies for processing real feedstock [11]. Once distilled, bioethanol contains various organic impurities, mostly fusel oil (propanol, butanol, pentanol, etc.) [11,12], which can adversely affect its further processing. In particular, 2G bioethanol derived from oat hulls [13,14] and *Miscanthus* [12,15] is contaminated with C3-alcohols in excess of 60% of the total fusel oil impurities. The effect of ethanol impurities has been widely discussed in relation to the steam reforming of ethanol into hydrogen [11,16–19]. It was shown in [16,17] that C3-alcohols of 1% mol reduce the feedstock conversion in ethanol steam reforming over alumina-based catalysts. Studies on the impact of ethanol impurities on ethylene production are very scarce. When evaluating the process of ethylene production from ethanol contaminated with organic impurities up to ~1% wt., Mohsenzadeh et al. [20] showed that impurities have no effect on the ethylene quality when the technology provides for conventional ethylene purification stages. However, this estimation did not address the impact of impurities on the activity and selectivity of the ethanol dehydration catalyst. In testing, ethylene

produced from a real 2G bioethanol contained less than 0.5 g/L (~0.05% mol) organic impurities [12], and a slight increase in ethylene selectivity due to suppression of byproducts formation without loss in catalyst activity was observed; however, no systematic study was carried out. The effect of 2-propanol (*i-PrOH*) impurity on ethylene production over an alumina catalyst was examined by varying the concentration and temperature [15], but no kinetic model was suggested.

Kinetic models with different levels of detail are used to describe catalytic processes of ethanol to ethylene dehydration (*EtOH*-to-*C2*). Detailed kinetic models that consider the inhibitory actions of water and ethanol as the main components of the reaction feedstock are discussed in [21–24]. Kagyrmanova et al. [25] employed semi-empirical power-law equations for product formation rates and showed a good agreement between the pilot-scale experiments and predicted data, which were used to simulate a commercial multi-tubular ethanol dehydration reactor. When modelling the ethanol dehydration, the formation routes of the target ethylene *C2* (1) and intermediate diethyl ether *DEE* (2–3) products are traditionally factored in, while for byproducts, only the formation of butylene *C4* (5) [26] or *C4* and acetaldehyde *AA* (4) [25,27] is considered. Other studies additionally take into account the formation of *COx* from *EtOH* [28] and ethane from *C2* [29].



A pilot study [21] demonstrated that *C4* could come from both *C2* (5) and *DEE* (6). In [21], ethane was observed among the *EtOH*-to-*C2* dehydration byproducts at high conversions, while the *AA* selectivity declined due to the *Cox* formation, as ethanol conversion rose above 98%. Thus, we can assume that the formation of *Cox* from *AA* is the main route (7). After removal of liquid reaction products (alcohols, aldehydes, esters), ethane remains one of the main gas products in dry-ethylene, which affects its quality [21]. Therefore, it is necessary to consider formation of ethane from *C2* by Reaction (8).



Propylene is the main product of *i-PrOH* dehydration (9) [15,30–32].



Diisopropyl ether is another product of *i-PrOH* dehydration; it was observed at temperatures below 300 °C [30–32]. However, in *EtOH* to *C2* dehydration performed at temperatures above 350 °C, conversion of C3-alcohols impurities leads to the formation of propylene only; other reaction products were not observed [15].

In the present work, we experimentally studied the impact of C3-alcohols impurities on ethanol dehydration to ethylene, as well as on the catalytic activity of a proprietary alumina catalyst [21]. To the best of our knowledge, an advanced kinetic model of dehydration of contaminated ethanol into ethylene, which takes into account the influence of C3-alcohols impurities on the formation of the target product, byproducts, and secondary reaction products, was first proposed. Mathematical simulation using the kinetic model allowed a preliminary assessment of the effect of impurities on ethylene production in a multi-tubular reactor (*MTR*).

2. Results

2.1. Experimental Results

Figures 1 and 2 show the results of an experimental study of the effect of C3-alcohols impurities on ethanol conversion X_A and products yield Y_i in the isothermal reactor by varying the temperature, anhydrous ethanol loading $LHSV_A$, and concentration of *n*-PrOH and *i*-PrOH under the reaction-controlled conditions. The Nomenclature is given in Appendix A.

In dehydration of both pure ($m0$) and contaminated with C3-alcohols ($m1$ – $m4$) ethanol at 350–400 °C and $LHSV_A$ of 96–27 h^{-1} , ethylene was the main product; its yield Y_{C2} reached 37–94% mol with X_A of 63–96% (Figures 1 and 2), yields of byproducts C4, AA, ethane, CO x were 0.3–2%, 0.03–1%, 0.2–0.6%, and 0.001–0.06% mol, respectively. C3-alcohol conversion (X_{PrOH}) was 22–99% (Figures 1 and 2). In the dehydration of C3-alcohols, no products, except for propylene, were observed; therefore, the conversion X_{PrOH} was equal to the propylene yield Y_{C3} .

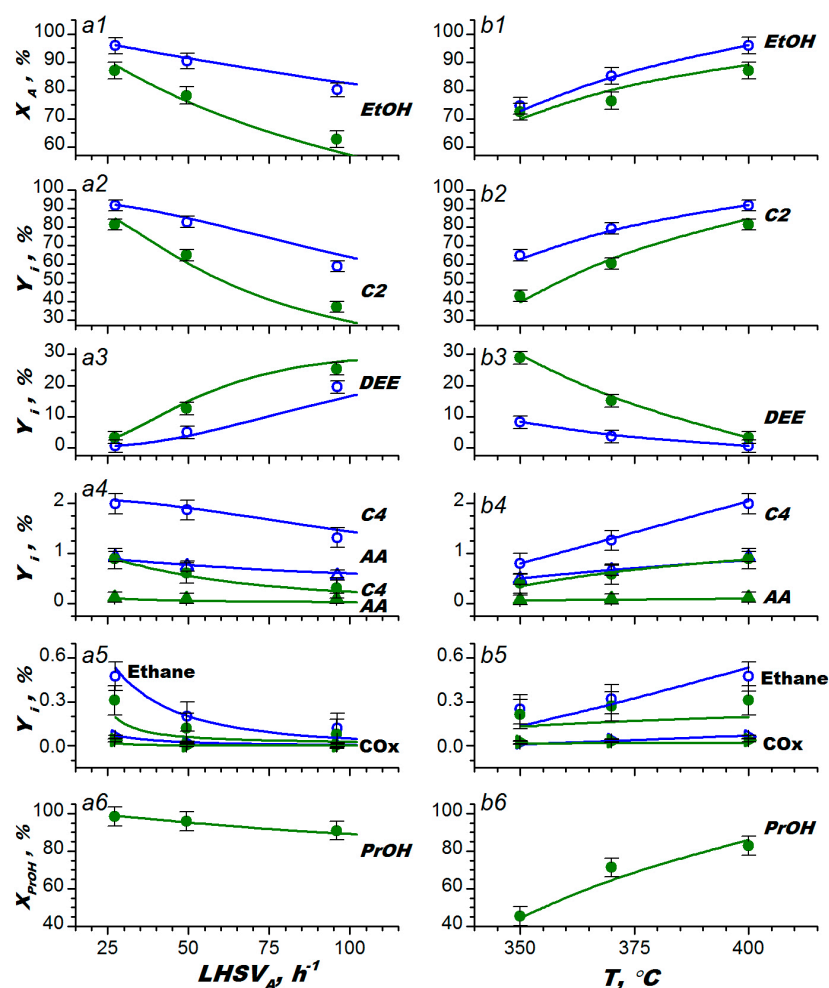


Figure 1. Effect of *n*-PrOH impurity in 92% wt feedstock on ethanol X_A and propanol X_{PrOH} conversions, and products yield Y_i with variation in $LHSV_A$ at 400 °C (a1–a6) and in T at $LHSV_A$ ~27 h^{-1} (b1–b6) for pure ethanol ($m0$, open), contaminated ethanol with *n*-PrOH of 0.01% ($m1$, semi-open) and 0.27% ($m3$, solid). C2, DEE, C4, ethane (circle), AA, and CO x (triangle). Conditions: PFR; proprietary Al_2O_3 catalysts of 0.25–0.50 mm. Symbols indicate experiments; lines indicate calculations for PFR using the extended kinetic model.

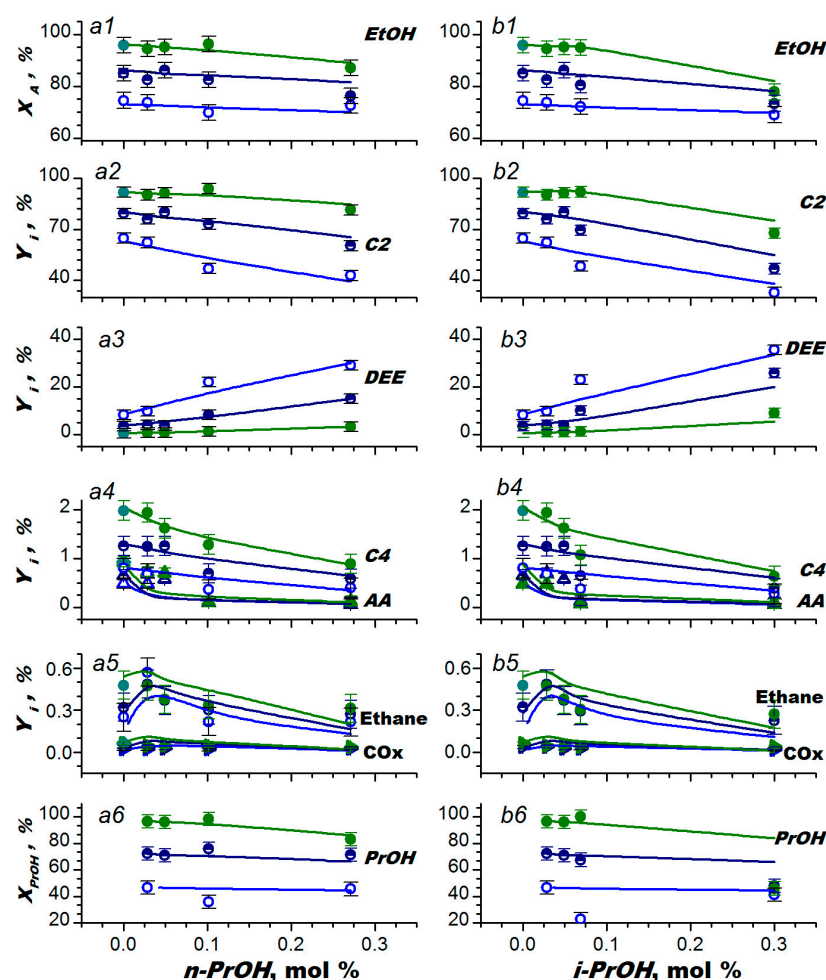


Figure 2. Effect of *n*-PrOH (a1–a6) and *i*-PrOH (b1–b6) impurity in 92% wt feedstock on ethanol X_A and propanol X_{PrOH} conversions, and products yield Y_i at 350 (open), 370 (semi-open), and 400 °C (solid). C2, DEE, C4, ethane (circle), AA, and COx (triangle). For conditions, see Figure 1. Symbols indicate experiments; lines indicate calculations for PFR using the extended kinetic model.

When pure ethanol m_0 was dehydrated at 400 °C, with an increase in $LHSV_A$ from 27 to 96 h^{-1} (Figure 1a), the Y_{C2} dropped by 36% mol with a 17% decrease in X_A , mainly due to a ~20% increase in Y_{DEE} ; the total yield of byproducts (C4, AA, ethane, COx) decreased by 1.5% mol. This indicates a parallel-consecutive scheme of C2 formation through DEE as an intermediate (1–3), i.e., routes of products formation directly from EtOH (1,2) dominate at lower X_A , and route of C2 formation from DEE (3) dominates at higher X_A .

Ethanol m_3 contaminated with *n*-PrOH of 0.27% gave the total yield of byproducts 2.5–5 times lower than that for m_0 , as shown in Figure 1(a4,a5). At higher X_A ($LHSV_A \sim 27 h^{-1}$), this impurity reduced Y_{C2} and X_A by 10% mol and increased Y_{DEE} by 4% mol (Figure 1(a1–a3)) compared to m_0 . Meanwhile, at lower X_A ($LHSV_A \sim 96 h^{-1}$), the impurity reduced Y_{C2} and X_A by 20% and kept ~4% mol increase for Y_{DEE} . As $LHSV_A$ increased, the conversion of impurity X_{PrOH} decreased by ~7% (Figure 1(a6)). Given the parallel-consecutive scheme of products formation, the observed difference in the product yields at lower and higher X_A may be related to the inhibitory effect of impurity on the direct routes of the products formation from EtOH (1). The slight change in Y_{DEE} with the significant decline in X_A may be due to impurity inhibition of the DEE consumption routes (3,6).

When we reduced the temperature by 50 °C at $LHSV_A \sim 27 h^{-1}$ for m_0 (Figure 1b), the values of X_A and Y_{C2} decreased by 20% and 27% mol, respectively, while Y_{DEE} rose by ~7% mol (Figure 1(b1–b3)); the total yield of byproducts decreased by 2% mol (Figure 1(b4,b5)). Thus, the temperature favors the yield of C2 rather than byproducts. Compared to m_0 ,

impurity of *n*-PrOH (*m*3) made an observed decrease in X_A and byproduct yields had a less steep temperature (Figure 1(b1,b4,b5)), and the decrease in Y_{C2} and Y_{DEE} was steeper (Figure 1(b2,b3)). This indicates that impurity of *n*-PrOH changes the temperature dependencies of the product formation rates and suppresses the *EtOH* consumption into C2 and DEE (1,2), and the DEE consumption into C2 (3). As the temperature was reduced, the X_{PrOH} decreased by ~35% (Figure 1(b6)).

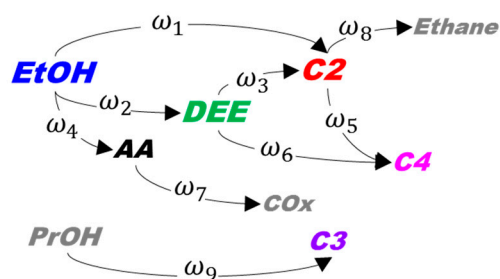
With the increase in *n*-PrOH and *i*-PrOH concentration (Figure 2(a6,b6)), C3-alcohols conversion X_{PrOH} declined by 1–9%. The highest content of byproducts was observed in the dehydration of pure ethanol: the yield of butylene was as high as 2% mol (Figure 2(a4,b4)), while the yields of AA (Figure 2(a2,b2)), ethane, and CO_x (Figure 2(a5,b5)) were as high as ~1, ~0.5, and ~0.06% mol, respectively. When dehydrating ethanol was contaminated with *n*-PrOH or *i*-PrOH, the total yield of byproducts was as low as ~0.7 or ~0.5% mol, respectively; this quality of ethylene was achieved at the highest concentration of C3-alcohols and the lowest temperature.

A 10-fold increase in impurity content, from 0.03 to 0.3% mol, reduces the yield of C2 and byproducts (C4, ethane, CO_x) by an average of ~1.4 and ~2.4 times, respectively, while the AA yield drops by ~7 times (Figure 2). However, at 400 °C, within the C3-alcohol concentration range of 0.05–0.1% mol, the highest values of X_A (96.2 and 95.1%) and Y_{C2} (94 and 92%) were observed (for *n*-PrOH and *i*-PrOH, respectively). Note that relative to X_A and Y_{C2} obtained at impurity concentrations of 0–0.03%, such excess is only 1–3% mol, which is not much larger than the experimental error in measuring X_A and Y_{C2} . In any case, there may be a narrow range of C3-alcohol concentrations, in which the impact of impurities is negligible, but it increases significantly with impurities greater than ~0.1% mol (Figure 2).

The effect of *n*-PrOH (Figure 2a) on X_A and Y_i is not very different from that of *i*-PrOH (Figure 2b). On the average, the dehydration indices (X_A and Y_i) decrease 1.3 times more in the presence of *i*-PrOH impurity.

2.2. Kinetic Model

The proprietary [21] and commercially available [25] alumina catalysts remained stable for 72 h when dehydrating 94–96% ethanol in a pilot-scale reactor [21,25], and were stable over a total time-on-stream (TOS) of 8–12 h when exposed to impurities (Section 4.1). This indicates that the alumina catalysts are sufficiently active in dehydration of azeotropic and contaminated ethanol, despite the presence of carbonaceous deposits on the catalyst surface noted in [33]. These facts allowed us to neglect the coke formation and assume steady-state conditions in the extended kinetic model for the *EtOH*-to-C2 process on the proprietary alumina catalyst. The reaction network of bioethanol dehydration is shown in Scheme 1.



Scheme 1. Reaction network.

Computer processing of the experimental data allowed us to propose a semi-empirical kinetic model for reactions rates, in which the coefficient β_j (10) formally accounted for the impact of C3-alcohol impurities on the product formation.

$$\beta_j = \frac{(1 + a_j P_{PrOH})}{(1 + b_j P_{PrOH})^2}, \quad (10)$$

here, $j = 1-9$; P_{PrOH} is the partial pressure of C3-alcohols; a_j and b_j are temperature dependent constants: $a_j = a_{0j} \cdot e^{-\frac{E_{aj}}{RT}}$, $b_j = b_{0j} \cdot e^{-\frac{E_{bj}}{RT}}$; a_{0j} and b_{0j} are the pre-exponential factors; E_{aj} and E_{bj} are the temperature coefficients in the Arrhenius equation.

The coefficient β_j is a formalized form of the kinetic equation where a_{0j} , b_{0j} , E_{aj} and E_{bj} are the generalized parameters describing the changes in the reaction rates of the product formation when exposed to a mixture of C3-alcohols impurities. In the suggested form, coefficient β_j can describe both the weak inhibition (and even acceleration) of the product formation rates at low impurity concentration, and the significant inhibition of the rates at high impurity concentration.

The reaction rate equations and its parameters are given in Table 1. The rate Equations (11)–(19) correspond to the stoichiometric Reactions (1)–(9), respectively. Kinetic model includes five reactions (11)–(15) discussed in [25,27], and four new reactions: formation of C4 from DEE (16), formation of carbon oxides (17) and ethane (18), and transformation of propanol (PrOH) impurities into propylene (19).

Table 1. Kinetic model and its parameters.

Reaction Rate Equations, ω_j	k_{0j} , $\frac{\text{mol}}{\text{atm}^n \cdot \text{kg} \cdot \text{s}}$	E_j , kJ/mol	Coefficient $\beta_j = \frac{(1+a_j P_{PrOH})}{(1+b_j P_{PrOH})^2}$			
			a_{0j}	E_{aj}	b_{0j}	E_{bj}
(11) $\omega_1 = k_1 P_{EtOH} \beta_1$	1.412×10^{10}	141.5	9.249×10^{17}	195.0	4.557×10^{18}	200.0
(12) $\omega_2 = k_2 P_{EtOH}^2 \beta_2$	7.434×10^9	125.1	3.127×10^{17}	187.0	6.025×10^{17}	191.0
(13) $\omega_3 = k_3 P_{DEE} \beta_3$	1.587×10^4	52.1	5.665×10^8	71.5	1.682×10^3	4.0
(14) $\omega_4 = k_4 P_{EtOH} \beta_4$	2.069×10^7	119.7	–	–	1.1×10^9	73.7
(15) $\omega_5 = k_5 P_{C_2}^2 \beta_5$	9.027×10^{-1}	63.6	–	–	2.258×10^4	18.5
(16) $\omega_6 = k_6 P_{DEE} \beta_6$	9.041×10^5	95.2	–	–	1.389×10^3	5.0
(17) $\omega_7 = k_7 P_{AA} P_{H_2O}^3 \beta_7$	1.950×10^{-2}	1.0	1.560×10^7	18.4	5.417×10^{10}	86.0
(18) $\omega_8 = k_8 P_{C_2} P_{H_2} \beta_8$	2.254×10^{-1}	1.0	1.672×10^{13}	105.0	5.634×10^3	48.0
(19) $\omega_9 = k_9 P_{PrOH} \beta_9$	1.331×10^9	120.0	–	–	8.452×10^{17}	200.0

ω_j is the rate of the j -th reaction under reaction-controlled conditions; P_i is the partial pressure of the i -th component of the reaction mixture; k_j is the kinetic constant governed by the Arrhenius law $k_j = k_{0j} \cdot e^{-\frac{E_j}{RT}}$; k_{0j} is the pre-exponential factor; E_j is the temperature coefficient, $R = 8.314 \frac{\text{J}}{\text{mol} \cdot \text{K}}$; n is reaction order; β_j is the coefficient that describes the effect of C3-alcohols impurities on ω_j . The rate Equations (11)–(19) correspond to the stoichiometric Reactions (1)–(9), respectively.

2.3. Validation of the Kinetic Model

Reagents concentrations measured in the isothermal plug-flow reactor (PFR) under reaction-controlled conditions correlate quite well with the values predicted by the kinetic model, as seen in Figure 3. In Figure 3a,b, the correlations for pure and contaminated ethanol are plotted against 32 experimental data points. Since the values of concentrations (Figure 3a,b) and yields of byproducts (Figure 3c) were much lower than those of ethylene, we therefore applied a scaling factor to display all substances on the same graph.

With the use of the extended kinetic model, the relative errors in calculation X_A and Y_i in PFR were in the ranges of 3–55% rel. for contaminated ethanol (Table 2, #1) and 1–11% rel. for pure ethanol (Table 2, #2). In evaluating small concentrations of side (C4, AA) and secondary (ethane, COx) products, the calculation errors are higher. In some cases, the calculation error may be due to the use of the coefficient β_j with generalized parameters in the kinetic model.

Before modeling the dehydration of contaminated ethanol in a large-scale commercial multi-tubular reactor (MTR), we compared the process indices in the MTR predicted using an extended kinetic model with the results of the experimental process study in a wall-heated pilot tubular reactor (10 data points in total); the latter were published in [21]. In the pilot studies, the calculation errors were in the range of 0.2–22% rel. for X_A and Y_i , except for Y_{COx} (Table 2, #3). Because of the small COx content (~0.002% mol), the error in calculation COx yield was 119% rel., which is much higher than for the other components.

A sufficient correlation between calculated values and experimental measurements in the pilot study is shown in Figure 3c.

The extended kinetic model proposed here provides an adequate description of the experimentally observed impact of the C3-alcohols on the conversion and yields of all reaction products in the *EtOH*-to-C2 dehydration process.

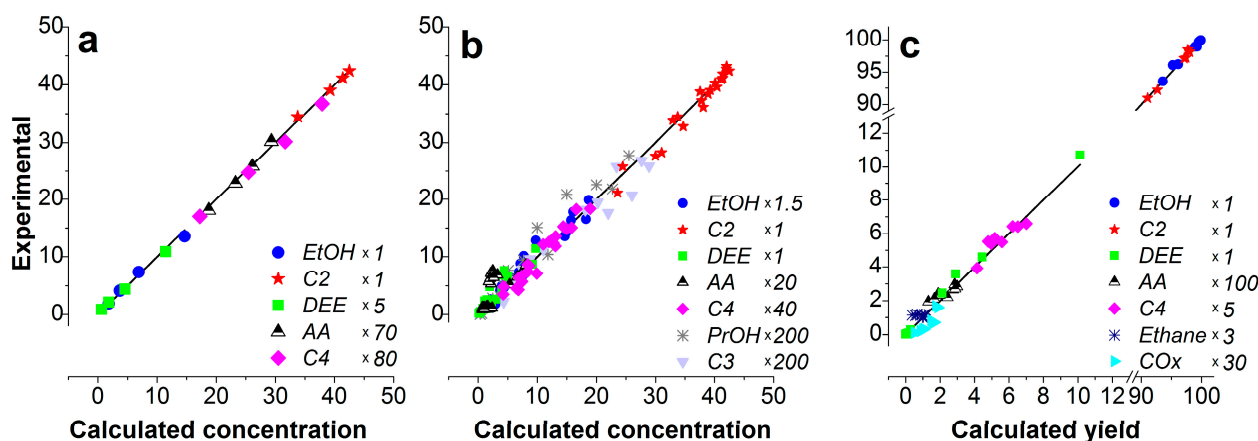


Figure 3. Correlation between the measured and calculated values. Reactor design: plug-flow (a,b), tubular with wall heating (c). Ethanol: pure (a,c), contaminated (b). In the legend, the numbers mean the scaling factors for each substance.

Table 2. Calculation errors.

#	Ethanol Grade	Reactor	Calculation Error, Percent Relative (% rel)							
			X_A	X_{PrOH}	Y_{C2}	Y_{DEE}	Y_{C4}	Y_{ethane}	Y_{AA}	Y_{COx}
1	Contaminated	Lab	3	5	5	14	12	46	22	55
2	Pure	Lab	1	—	1	7	3	9	3	11
3	Pure	Pilot	0.2	—	0.3	12	2	22	11	119

2.4. Dehydration of Contaminated Bioethanol to Ethylene: Simulating Procedure

2.4.1. The Process in Plug-Flow Reactor (PFR) under Reaction-Controlled Conditions

The process indices calculated using the extended kinetic model (Table 1, Equations (11)–(19)) made it possible to evaluate the effect of C3-alcohols on the products formation routes. We simulated dehydration of bioethanol contaminated with C3-alcohols of 0.001, 0.15 and 0.3% mol in *PFR* at 400 °C. Figure 4 illustrates how the selectivity (a) and yield (b) of C2 and DEE depend on ethanol conversion X_A . Byproduct selectivity is given in Supplementary, Figure S1.

If we compare the selectivity at $X_A \approx 1\%$ conversion, we can assess the effect of C3-alcohols on the rates of products formation directly from *EtOH* (Figure 4a). At $X_A \approx 1\%$ the S_{C2} and S_{DEE} were 5.5–2.5 and 94–97% mol, respectively; therefore, C2 is obtained mainly via the consecutive route $EtOH \rightarrow DEE \rightarrow C2$ (2,3). This can be clearly seen in Figure 4b, where Y_{DEE} passes through the maximum at $X_A \sim 48$ –57%. As calculated, the C3-alcohol impurities have a minimal effect on the formation of DEE from *EtOH* (12). With the impurity increase from 0.001 to 0.3%, DEE selectivity at $X_A \approx 1\%$ becomes $\sim 3\%$ mol higher (Figure 4a), resulting in a slight increase in C2 formation via the consecutive route (2,3). C3-alcohol impurities lead to a growth in S_{C2} and Y_{C2} at X_A above 20% (Figure 4) but require a decrease in $LHSV_A$ to achieve the same X_A as in pure ethanol dehydration. Thus, at $X_A \approx 93.6\%$ for ethanol contaminated with impurities of 0.001–0.03 and 0.3% mol, S_{C2} of 94.6 and 97.6%, and Y_{C2} of 88.5 and 91.4% were achieved at $LHSV_A$ of 39 and 16.5 h^{-1} , respectively.

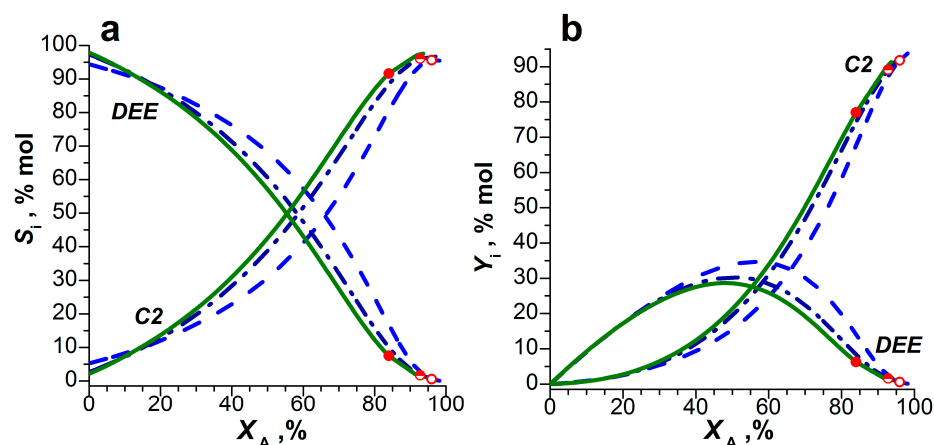


Figure 4. The calculated C2 and DEE selectivity (a) and yield (b) vs. ethanol conversion X_A in PFR. Conditions: 400 °C, 1.2 g catalyst, 21.05 g/h solution of 92% wt EtOH and C3-alcohol impurities of 0.001 (dash, open), 0.15 (dash-dot, half), and 0.3% mol (solid, solid). Symbols indicate S_i and Y_i at $LHSV_A \approx 27 \text{ h}^{-1}$.

Figure 5 shows how coefficient β_j varies with increasing C3-alcohol concentration in bioethanol samples. It follows from the expression (10) for coefficient β_j that if P_{PrOH} tends to zero, the coefficient β_j tends to unity, that is, the inhibition of reaction rates of product formation by impurities is less pronounced.

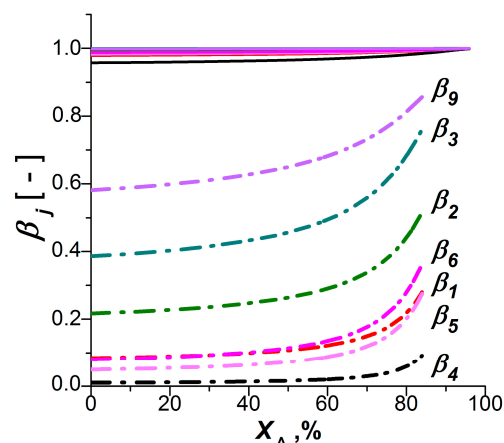


Figure 5. The coefficient β_j vs. ethanol conversion X_A in PFR. Conditions as in Figure 3. C3-alcohol of 0.001 (solid) and 0.3% mol (dash-dot).

When dehydrating bioethanol with 0.001% mol C3-alcohols, the coefficients β_j were equal at least to 0.96; i.e., low concentration of impurity had almost no effect on the products formation in EtOH-to-C2 process (Figure 5, solid lines). When dehydrating bioethanol with 0.3% mol C3-alcohols, the lowest $\beta_4 = 0.08$ –0.3 was found for AA formation by Reaction (14), and the highest was $\beta_9 = 0.6$ –0.9 for PrOH conversion by Reaction (19). This means that AA formation is strongly affected by impurities, while inhibition of PrOH conversion is less pronounced (Figure 5, dash-dot lines). The inhibitory effect of C3-alcohols on the formation of different products varies greatly; thus, at 0.3% mol and $X_A \sim 50\%$, the formation rates of AA (14), C4 (15, 16), and C2 (11) decreased by factors of ~ 60 , 9–13, and 9 ($1/\beta_j$), while the formation rate of DEE (12) and its consumption to C2 (13) decreased by factors ~ 3.8 and 2, respectively. The production of C4 from DEE and from C2 (5, 6), and C2 directly from EtOH (1) is inhibited almost equally, as evidenced by the close values of β_1 , β_5 , and β_6 (Figure 5).

2.4.2. The Process in Multi-Tubular Reactor (MTR)

In this study, we focused only on the main process features that occur during dehydration in *MTR* of ethanol contaminated with C3-alcohols.

First, we found the dehydration process conditions (heat-medium temperature T_W , linear velocity U , bed height L , tube diameter D) that ensure the maximum Y_{C2} when pure ethanol is used. A diluted 92% ethanol, the quality of which corresponded to the quality of a real bioethanol (Section 4.1), was considered as a feedstock. The parameters T_W , U , L , and D were varied in the range of 420–450 °C, 0.85–1.2 m/s, 2.5–4.5 m, and 30–34 mm, respectively; number of tubes N was adjusted to provide ethylene capacity of 60 KTPA (25).

The indices of selectivity S_i , product yield Y_i , and ethylene quality Q_{C2} (26), plotted as a function of ethanol conversion X_A , are shown in Figure 6. In *MTR*, when L extends from 2.5 to 3.5 m, X_A increases from 98.5 to 99.99%. The process indicators at the reactor outlet calculated at a fixed L are provided in Table 3. The temperature T_W favors selectivity for ethylene rather than for byproducts (Figure 6); this is consistent with the *PFR* experiments presented above in Figure 1b, and with the pilot experiments reported in [21].

In dehydrating pure 92% ethanol, the maximum ethylene yield $Y_{C2} = 98.1\%$ was achieved when X_A was close to 99.9% (Figure 6c); the process conditions were as follows: $U = 0.85$ m/s, $T_W = 430$ °C, $D = 32$ mm, and $L = 3.5$ m. A further rise in conversion degree leads to a sharp drop in ethylene yield, mainly due to the formation of byproducts such as C4, ethane, and CO_x . In addition, ethylene quality drops dramatically if X_A rises above 99.8–99.9% (Figure 6d).

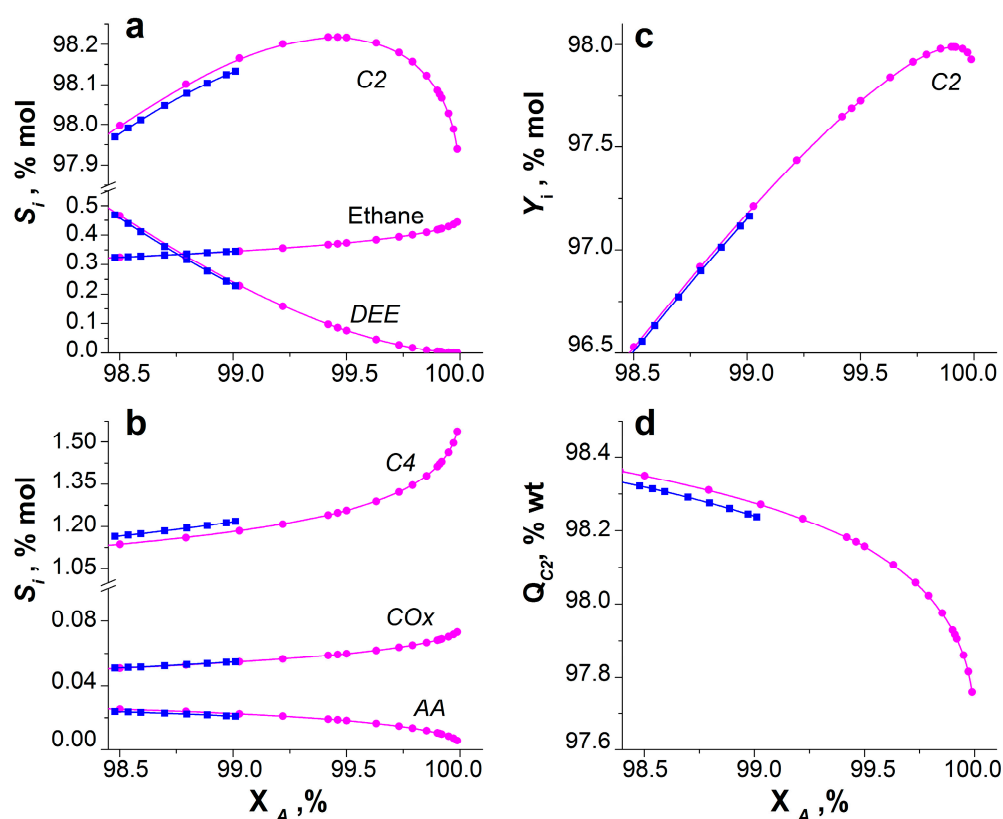


Figure 6. Selectivity S_i (a,b), yield Y_{C2} (c), and C2 fraction in dry-ethylene Q_{C2} (d) vs. conversion X_A in *MTR* under diffusion-controlled conditions. Conditions in Table 3: #1 (■), #2 (●).

Table 3. Dehydration of pure 92% ethanol in MTR over proprietary 6mm ring-shaped alumina catalyst.

#	Operating Conditions and Reactor Design Parameters						S_i , mol%						CI_{raw} , g/kg		
	U m/s	T_W , °C	D mm	L m	N 10^3 pcs	$LHSV_A$, h^{-1}	Y_{C2} , mol%	X_A , %	$C2$	DEE	$C4$	<i>Ethane</i>		<i>AA</i>	CO_x
1 (■)	1.0	420	30	3.0	3.0	2.6	97.2	99.0	98.13	0.23	1.22	0.35	0.02	0.05	1.83
2 (●)	0.85	430	32	3.5	3.0	1.9	98.0	99.9	98.06	0.00	1.43	0.42	0.01	0.07	1.81

U —linear velocity; T_W —heat-medium temperature; D —tube diameter; L —bed height; N —number of tubes.

Second, we have assessed the effect of C3-alcohols impurities on the performance of contaminated 92% ethanol dehydration process in *MTR* at the process parameters mentioned above ($U = 0.85$ m/s, $T_W = 430$ °C, $D = 32$ mm, $L = 3.5$ m).

The catalytic process on the ring-shaped granules is controlled by diffusion. In contrast to the process on small particles, C3-alcohols impurities have almost no effect on dehydration of contaminated ethanol in *MTR* on industrial size catalyst granules. Even at C3-alcohol concentration up to 3% (Section 4.3), X_A and Y_{C2} do not markedly change. Therefore, to discuss the results of modeling, we chose the indices of feedstock consumption CI_A and CI_{raw} (24), products capacity $P'C2$ (25), and dry-ethylene composition Q_i (Figure 7). The weak impact of impurities on X_A and Y_i is manifested by a slight decline in the anhydrous-ethanol consumption index CI_A (Figure 7a). When C3-alcohols are added to the feed in amounts up to 3% mol, the ethanol concentration becomes 2.4% mol lower (Section 4.3), while the yield of propylene as a product of C3-alcohols dehydration rises; this increases feed consumption index CI_{raw} (Figure 7a) and decreases production capacity $P'C2$ by ~3% rel. (Figure 7b). An ~5% wt increase of propylene concentration means a corresponding loss in the amount of C2 in dry-ethylene from 98 to 93% wt (Figure 7c). In order to raise the ethylene productivity to the required 60 KTPA, either the number of tubes in *MTR* or the temperature T_W should be increased.

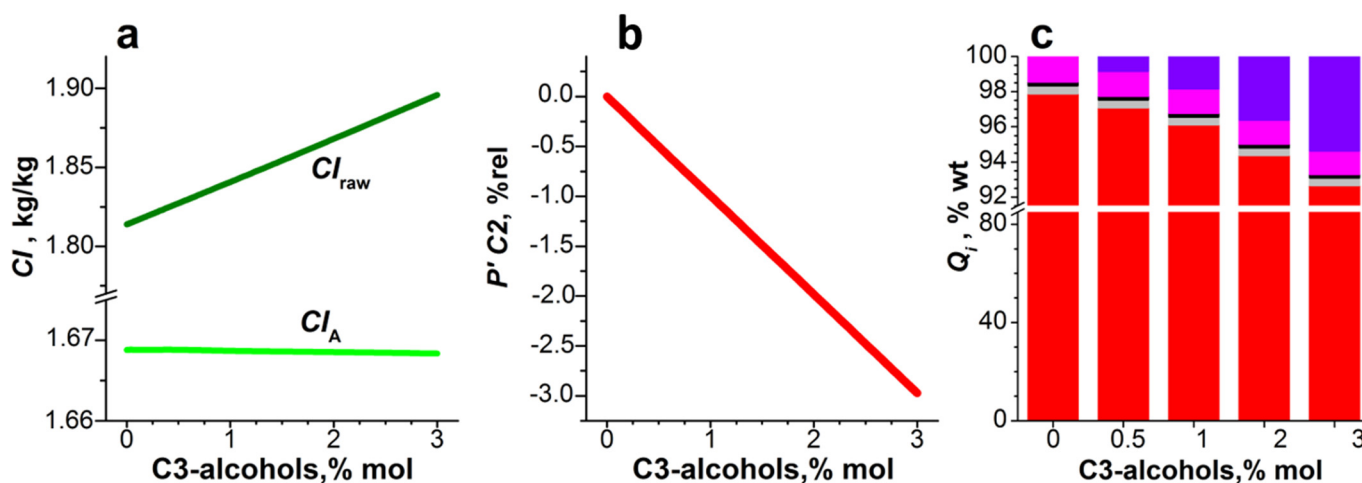


Figure 7. The impact of impurity concentrations on feedstock consumption (a), products capacity (b) and dry-ethylene quality (c) for *EtOH*-to-*C2* process in the *MTR*. Conditions: #2 in Table 3. ■—propylene, ■—C4, ■—COx, ■—ethane, and H₂, ■—C2.

3. Discussion

Our experimental data showed that C3-alcohols in concentrations below 0.1% mol have almost no negative effect on product formation, but amounts above 0.1% mol strongly inhibit the formation of by-products, and this is most true for the formation of AA. Of the C3-alcohols, the branched isomer has a greater effect on *EtOH*-to-*C2* conversion; this observation is consistent with the data reported in [16]. The resulting set of experimental data served as a basis for the formulation of the kinetic model.

As observed experimentally, the total yield of C2 and DEE exceeds the total yield of byproducts (Figures 1 and 2). When X_A is varied, the yields of C2 and DEE change significantly and in opposite directions; contrary to them, the by-product yields change only slightly. This behavior is consistent with the parallel-consecutive network of C2 formation and allows us to assume that the consecutive path of C2 formation via DEE predominates. It follows that impurities suppress the conversion of *EtOH* to DEE and its subsequent conversion to C2; this is the main reason for the decrease in X_A .

Modelling the *PFR* using the kinetic model (11–19) showed that ethylene formation through DEE by consecutive route (2,3) prevails over parallel route (1); this confirms the experimental observations outlined above. Impurities inhibit the direct route of ethylene

formation ($1/\beta_1 \approx 9$) more strongly than the consecutive one ($1/\beta_2 \approx 3.8$, $1/\beta_3 \approx 2$), which increases the contribution of consecutive route to ethylene accumulation. Reduction of catalyst activity during dehydration of contaminated ethanol can be explained by the suppression of the predominant routes of *DEE* formation and consumption (2,3). The impurities also significantly inhibit the formation of by-products ($1/\beta_j \approx 9$ –60); with equal conversions of contaminated and pure ethanol this could give ~3% mol higher ethylene yield but would require more than a twofold reduction in the feedstock load $LHSV_A$. The values of the β_j coefficient are close for the routes of butylene formation from C2 (5) and from *DEE* (6), as well as for ethylene formation from *EtOH* (1) ($1/\beta_1 \approx 1/\beta_5 \approx 1/\beta_6 \approx 9$ –13); this may indicate that these products are formed with the participation of the same active sites. Undoubtedly, this assumption requires additional experimental research.

Simulated data for *MTR* showed that the influence of C3-alcohols impurities on the ethanol dehydration in the *MTR* was significantly less than in the *PFR*. The reason may be that the apparent kinetics shifts from being dominated by the chemical reactivity on the fine-dispersed catalyst to the internal diffusion controlled on the catalyst grains. This leads to a decrease in the observed reaction rates, including the rates of formation of byproducts; we can say that the diffusion inside the grains levels out the effect of impurities on the dehydration process.

The negative effect of C3-alcohols on the process performance in *MTR* can be caused mainly by dilution of ethanol with impurities and formation of propylene. The first factor leads to a lower ethylene production capacity, while the second one reduces the quality of ethylene produced. However, for a given *MTR* size, the slight (~3% rel.) decrease in ethylene capacity can easily be compensated by raising temperature T_W by 2–5 degrees; the standard crude-ethylene conditioning shall give a target polymer-grade product [20]. Since the influence of impurities during dehydration of the real (contaminated) bioethanol is insignificant, it is possible to save the costs of the raw purification and thereby reduce the cost of processing of real bioethanol into ethylene. This assumption needs to be confirmed experimentally on a pilot scale.

4. Materials and Methods

4.1. Experimental

The catalytic dehydration of ethanol to ethylene was run in an isothermal flow reactor 12 mm in diameter on a catalyst with a particle size of 0.25–0.50 mm under reaction-controlled conditions [21]; the procedure and the main reactor features were reported in [12,15,21]. The catalyst bed was diluted with quartz grit at a 2:1 ratio. The catalyst particles were prepared by grinding the ring-shaped granules. The proprietary catalyst comprises a mixture of phases: 53% γ - Al_2O_3 and 47% χ - Al_2O_3 ; BET surface area was 208 m²/g. The textural and acidic properties of the catalyst, alkaline content, and preparation procedure were reported in [21].

Earlier, we found that in the real bioethanol derived from oat hulls and *Miscanthus* by the method described in [12–15], impurities of C3-alcohols prevail, their concentration reaches ~4 g/L, and the mass content of ethanol is ~92%. In the present study, we used two samples of a real *Miscanthus*-derived bioethanol (*b1* and *b2*), and five model samples prepared from a commercially available azeotropic ethanol diluted with distilled water and C3-alcohols, namely: pure (*m0*), contaminated with *n*-*PrOH* (*m1* and *m3*), and contaminated with *i*-*PrOH* (*m2* and *m4*). The composition of impurities in all samples expressed on anhydrous alcohol basis (g/L) is shown in Figure 8.

The effect of temperature (350–400 °C) and the concentration of C3-alcohols (0.03–0.3% mol) on the catalytic process was studied at 21 ± 0.05 g/h alcohol solution ($91.8 \pm 0.7\%$ wt *EtOH*) flow rate and 0.726 ± 0.005 g catalyst charge; anhydrous ethanol feed per catalyst volume $LHSV_A$ was $\sim 27.2 \pm 0.2$ h⁻¹. By changing the load of both the alcohol solution and the catalyst in the range of 21–33 g/h and 0.73–0.33 g, respectively, the $LHSV_A$ can be varied in the range of ~ 27.2 –96.1 h⁻¹. The effect of $LHSV_A$ on the catalytic

dehydration of pure ($m0$) and contaminated ($m3$) ethanol was studied at 400 °C. The total pressure in the reactor was 1.03–1.07 bar.

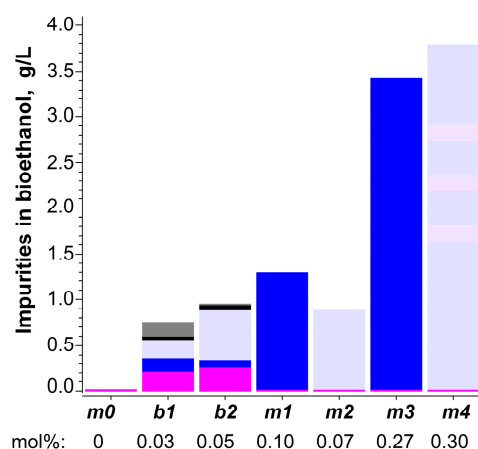


Figure 8. Impurities in the samples: pure ethanol ($m0$), real bioethanol ($b1$, $b2$), model ethanol contaminated with n -PrOH ($m1$, $m3$), same, contaminated with i -PrOH ($m2$, $m4$). Impurities: AA (■), methanol (■), i -PrOH (■), n -PrOH (■), isobutanol (■). The molar percentage of C3-alcohol in the gas phase is given below.

Product yield Y_i , ethanol conversion X_A , and product selectivity S_i were calculated by the Formulas (20)–(22).

$$Y_i = 100 \frac{\Delta m_i / \zeta_{ij}}{m_{EtOH} + \sum \Delta m_i / \zeta_{ij}}, \quad (11)$$

$$X_A = \sum Y_i, \quad (12)$$

$$S_i = \frac{Y_i}{X_A}, \quad (13)$$

here, Δm_i is the difference in molar fluxes of the i -th component at the reactor inlet and outlet, mol/h; ζ_{ij} is the stoichiometric coefficient of the i -th component in the j -th reaction; m_{EtOH} is the molar flux of ethanol at the reactor exit, mol/h.

To check the reproducibility and determine the experimental error, a series of experiments were performed for pure and contaminated ethanol under standard conditions. The relative experimental errors (rel.%) in measuring ethanol X_A and propanol X_{PrOH} conversions, and the yields of C2, DEE, C4, AA, ethane, and CO x were 2, 3, 3, 10, 12, 12, 32, and 17%, respectively. Resource tests were conducted under steady-state conditions while dehydrating either pure 92% wt ethanol, or ethanol contaminated with C3-alcohols, and each test lasted 8 h. The process indicators Y_i , X_A , S_i and mass balance were checked every 1–2 h during the catalyst time-on-stream. The mass balance for the entire series of measurements was $100 \pm 5\%$. The catalyst was stable within the measurement error.

4.2. Kinetic Modeling

The parameters of the kinetic model were determined using MathCad software by minimizing the deviations in the measured and calculated data for PFR; the procedure involved two main steps:

1. Determination of parameters k_j and E_j of the extended kinetic model for pure ethanol ($P_{PrOH} = 0$, $\beta_j = 1$);
2. Determination of the β_j parameters (a_{0j} , b_{0j} , E_{aj} , and E_{bj}) of the extended kinetic model for contaminated ethanol, with k_j and E_j found in the previous step. Real bioethanol contains a mixture of C3-alcohols in various ratios; therefore, the estimation of the generalized parameters of β_j (for a sum of n -PrOH and i -PrOH) seems more relevant. The upper limit of the parameters E_{aj} and E_{bj} was set as 200 kJ/mol.

4.3. Mathematical Modeling

A mathematical simulation using an extended kinetic model of dehydration of contaminated ethanol into ethylene allowed us to preliminarily assess how the impurities affect the performance of the process in the *MTR* [25].

For this purpose, we used the two-dimensional quasi-homogeneous model of the wall-heated tubular reactor; this model had been reported in [27,34]. The model includes differential equations for material and heat transport in the radial and axial directions in the bed (Supplementary Materials), and considers the different interstitial gas velocities around ring-shaped grains and inside their holes (Figure S2), as well as the equation describing diffusion and reactions in the porous isothermal catalyst grain (23):

$$\frac{\partial}{\partial \rho} \left(D_{ri}^* \frac{\partial C_i}{\partial \rho} \right) - \frac{RT}{P} \frac{\partial}{\partial \rho} (V_i^* C_i) = \sum_{j=1}^9 \xi_{ij} \omega_j, \quad i = \overline{1, 11}, \quad (14)$$

here D_{ri}^* and V_i^* are the Wilke diffusion coefficient and hydrodynamic velocity of the i -th component; C_i is the molar concentration of the i -th component; ω_j is the rate of the j -th reaction under reaction-controlled conditions; ω_j is the apparent rate of the j -th reaction in the catalyst grain defined as $\frac{1}{\rho_{grain}} \int_0^{\rho_{grain}} \omega_j(\rho) d\rho$; ρ_{grain} is the equivalent grain size, i.e., the ratio of the geometric volume to the external geometric surface area.

The Wilke diffusion coefficient D_{ri}^* and hydrodynamic velocity V_i^* [34] depend on the effective binary diffusion coefficient $D_{ik}^* = \Pi D_{ik}$ and on the effective Knudsen diffusion coefficient $D_i^{*kn} = \Pi D_i^{kn}$, where D_{ik} is binary diffusion coefficient, D_i^{kn} is Knudsen diffusion coefficient, and Π is the empirical permeability coefficient accounting for the physical behavior of the porous structure ($\Pi \approx 0.2$).

In the present study, the behavior of *MTR* during the dehydration of 92% wt. pure and contaminated ethanol over a ring-shaped catalyst was simulated. The strength of ethanol corresponded to the strength of a real bioethanol (Section 4.1). The catalyst dimensions (diameter \times height \times wall thickness = 6.0 \times 5.30 \times 1.25 mm) were set as the average sizes of the ring-shaped grains used in the pilot studies [21], where the heat-medium temperature T_W , linear velocity U , and bed height L were varied at a fixed tube diameter D . The change in U and L led to a variation in the feedstock loading per catalyst volume, $LHSV_A$, in terms of anhydrous ethanol. The concentration of C3-alcohols impurities in gas feed varied from 0.5 to 3% mol (which is equivalent to ~ 0.6 to 30 g/L per anhydrous ethanol); the molar composition of the inlet gas mixture is depicted in Figure 9. *MTR* simulation for 60 KTPA ethylene capacity was performed assuming an identical behavior for all tubes.

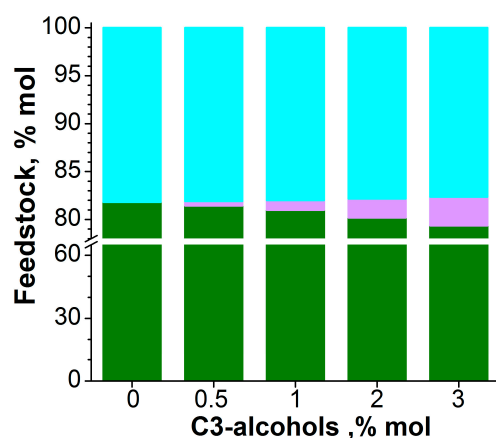


Figure 9. Feedstock composition for *MTR* plotted against C3-alcohol concentrations in bioethanol.

To validate the model adequacy, we compared the results of our previous pilot studies for pure ethanol published in [21] with the data simulated by the 2D mathematical model using the new extended kinetic model (Section 2.2) for the wall-heated tubular reactor.

The simulation of the process took place in two stages:

1. Determination of process conditions (T_W , U) and reactor design (L , D , N) to achieve maximum ethylene yield from pure (not contaminated) 92% ethanol and to ensure ethylene capacity of 60 KTPA;
2. Determination of process indicators when varying the impurity concentrations in the *MTR* under process conditions and reactor design defined in the previous step.

Indicators of the catalytic process, namely ethylene yield Y_{C2} , consumption indices of anhydrous ethanol and feedstock (CI_A and CI_{raw} kg/kg), relative ethylene production capacity ($P'C2$, rel.%), and weight fraction of $C2$ in dry-ethylene (Q_{C2} , wt%) were calculated by the Formulas (24)–(26):

$$CI_A = \frac{f_{EtOH}}{f_{C2}} = \frac{100 \cdot 46}{Y_{C2} \cdot 28}, CI_{raw} = \frac{100 \cdot CI_A}{M_{EtOH}}, \quad (15)$$

$$P'C2 = \frac{PC2_{pure} - PC2_{contaminated}}{PC2_{pure}} \cdot 100, PC2 = \frac{f_{C2} \cdot N \cdot 8000}{10^6}, N = \frac{60 \text{ KTPA}}{f_{C2} \cdot 8000 \cdot 10^{-3}} \quad (16)$$

$$Q_{C2} = \frac{f_{C2}}{f_{C2} + f_{C3} + f_{H_2} + f_{ethane} + f_{CO_x} + f_{C4}} \cdot 100, \quad (17)$$

here, f_{C2} , f_{C4} , f_{ethane} , f_{CO_x} , f_{H_2} , and f_{C3} are the mass fluxes of ethylene, butylene, ethane, carbon oxides, hydrogen, and propylene, respectively, at the outlet of the single tube in *MTR*, kg/h; M_{EtOH} is the mass fraction of ethanol in the feed, % wt; $PC2$ is the ethylene production capacity of *MTR* in the dehydration of pure or contaminated ethanol, KTPA; N is the number of tubes to secure 60 KTPA with a pure ethanol as a feedstock, 10^3 pieces; 8000 is the annual operating time, h.

5. Conclusions

During experimental and theoretical studies on the dehydration of 92% bioethanol over alumina catalysts, how the content of C3-alcohols impurities in the feed affects the products selectivity and yield was quantitatively estimated. For the first time, an extended kinetic model of real ethanol dehydration has been proposed; it considers the influence of C3-alcohols impurities on the rates of formation of basic (ethylene and ether), side (butylene and acetaldehyde), and secondary (ethane and CO_x) reaction products.

The kinetic model has been approved experimentally in the dehydration of pure and contaminated ethanol on a milled catalyst in a plug-flow reactor, as well as in the dehydration of pure ethanol on a ring-shaped catalyst in a wall-heated tubular reactor.

C3-alcohols have very little effect on the process performance in *PFR* at concentrations below 0.05% mol; at higher loads they suppress the formation of byproducts by 9–60 times and ethylene formation directly from ethanol by 9 times, while ethylene formation via ether was only suppressed 2–3.8 times. Ethylene formation via ether is dominated on the tested catalyst. The branched propanol affects the ethanol-to-ethylene process more strongly than the linear isomer.

For the first time, to preliminarily assess the dehydration of contaminated ethanol in the *MTR*, we applied a quasi-homogeneous 2D model that incorporated an extended kinetic model. When ethanol conversion degree is 99.9%, the highest ethylene yield is 98.1%. Internal diffusion levels out the negative effect of C3-alcohols on the ethylene yield in the *MTR*. Despite this, ethylene productivity and its grade are reduced because impurities dilute ethanol and produce propylene. A proper adjustment of the heat-transfer fluid temperature and/or the number of tubes in the commercial *MTR* can provide the targeted ethylene production capacity.

Since the role of impurities in the catalytic dehydration process is very diverse, further in-depth studies of the influence of this important factor are necessary.

Supplementary Materials: The following supporting information can be downloaded at: <https://www.mdpi.com/article/10.3390/catal13030509/s1>, Mathematical model of the wall-heated tubular reactor; Figure S1: The calculated selectivity to C2, DEE, C4, AA, ethane and CO_x vs. ethanol conversion in PFR; Figure S2: A sketch of “gas flow sharing” in a holed cylinder. References [35–41] are cited in the Supplementary Materials.

Author Contributions: Conceptualization, E.V.O. and V.A.C.; methodology, E.V.O. and S.P.B.; validation, E.V.O., S.P.B. and M.A.K.; investigation, S.P.B. and M.A.K.; writing—original draft preparation, E.V.O. and S.P.B.; writing—review and editing, E.V.O. and V.A.C.; visualization, E.V.O.; project administration, E.V.O. All authors have read and agreed to the published version of the manuscript.

Funding: This work was supported by the Ministry of Science and Higher Education of the Russian Federation within the governmental order for Boreskov Institute of Catalysis (project AAAA-A21-121011390010-7).

Data Availability Statement: Not applicable.

Acknowledgments: The authors are grateful to Vernikovskaya N.V. for adapting the software package for calculating MTR using the new extended kinetic model.

Conflicts of Interest: The authors declare that they have no known competing interest or personal relationships that could have appeared to influence the work reported in this paper.

Appendix A. Nomenclature and Abbreviations

Components of the reaction mixture	
AA	Acetaldehyde, C ₂ H ₄ O
C2	Ethylene, C ₂ H ₄
C3	Propylene, C ₃ H ₆
C3-alcohols	<i>n</i> -PrOH and <i>i</i> -PrOH
C4	Butylene, C ₄ H ₈
DEE	Diethyl ether, (C ₂ H ₅) ₂ O
EtOH	Ethanol, C ₂ H ₅ OH
<i>n</i> -PrOH	1-Propanol, C ₃ H ₇ OH
<i>i</i> -PrOH	2-Propanol, C ₃ H ₇ OH
Samples of ethanol	
<i>b1, b2</i>	Bioethanol from <i>Miscanthus</i>
<i>m0</i>	Pure ethanol
<i>m1, m3</i>	Model bioethanol contaminated with <i>n</i> -PrOH
<i>m2, m4</i>	Model bioethanol contaminated with <i>i</i> -PrOH
Parameters of kinetics equation	
P_i	Partial pressure of the <i>i</i> -th component of the reaction mixture, atm
E_j	Temperature coefficient in Arrhenius equation, kJ·mol ⁻¹
k_j	Kinetic rate constant in ω_j , mol·atm ⁻ⁿ ·kg ⁻¹ ·s ⁻¹
k_{0j}	Pre-exponential factor in Arrhenius equation, mol·atm ⁻ⁿ ·kg ⁻¹ ·s ⁻¹
ω_j	Rate of the <i>j</i> -th reaction, mol·atm ⁻ⁿ ·kg ⁻¹ ·s ⁻¹
β_j	Coefficient considering the effect of C3-alcohols impurities on ω_j
Process indicators	
PFR	Plug-flow reactor
MTR	Multi-tubular reactor
CI_A	Consumption index of anhydrous ethanol, kg·kg ⁻¹
CI_{raw}	Consumption index of feedstock, kg·kg ⁻¹
D	Diameter of tube, mm
L	Height of catalyst bed, m
$LHSV_A$	Liquid hourly space velocity of anhydrous ethanol, h ⁻¹
N	Number of tubes, 10 ³ pieces
PC2	Productivity of ethylene, KTPA (thousand tons per year)
$P'C2$	Relative ethylene production capacity, % rel
$QC2$	Quality of ethylene (weight fraction of C2 in dry-ethylene), % wt.

S_i	Selectivity to the i -th product, % mol
T_W	Heat-medium temperature, °C
U	Linear velocity (STP), m/s
X_A	Conversion of anhydrous ethanol, %
X_{PrOH}	Conversion of C3-alcohols, %
Y_i	Yield of the i -th product, % mol

References

- Hulea, V. Toward Platform Chemicals from Bio-Based Ethylene: Heterogeneous Catalysts and Processes. *ACS Catal.* **2018**, *8*, 3263–3279. [\[CrossRef\]](#)
- Zacharopoulou, V.; Lemonidou, A. Olefins from Biomass Intermediates: A Review. *Catalysts* **2018**, *8*, 2. [\[CrossRef\]](#)
- Alvarenga, R.A.F.; Dewulf, J. Plastic vs. Fuel: Which use of the Brazilian ethanol can bring more environmental gains? *Renew. Energy* **2013**, *59*, 49–52. [\[CrossRef\]](#)
- Sharada, D.; Naresh, U.; Shiva, K.V.; Kumar, R.J. Drop-in plastics. In *Advanced Catalysis for Drop-in Chemicals*; Sudarsanam, P., Li, H., Eds.; Elsevier: Amsterdam, The Netherlands, 2022; pp. 31–46. [\[CrossRef\]](#)
- Khabusheva, E.M.; Krasnikov, D.V.; Goldt, A.E.; Fedorovskaya, E.O.; Tsapenko, A.P.; Zhang, Q.; Kauppinen, E.I.; Kallio, T.; Nasibulin, A.G. Joint effect of ethylene and toluene on carbon nanotube growth. *Carbon* **2022**, *189*, 474–483. [\[CrossRef\]](#)
- Ahmad, S.; Ding, E.-X.; Zhang, Q.; Jiang, H.; Sainio, J.; Tavakkoli, M.; Hussain, A.; Liao, Y.; Kauppinen, E.I. Roles of sulfur in floating-catalyst CVD growth of single-walled carbon nanotubes for transparent conductive film applications. *Chem. Eng. J.* **2019**, *378*, 122010. [\[CrossRef\]](#)
- Karagedov, G.R.; Shutilov, R.A.; Kolesov, B.A.; Kuznetsov, V.L. The effect of carbon nanotubes introduction on the mechanical properties of reaction bonded boron carbide ceramics. *J. Eur. Ceram. Soc.* **2021**, *41*, 5782–5790. [\[CrossRef\]](#)
- Barabashko, M.S.; Drozd, M.; Szewczyk, D.; Jeżowski, A.; Bagatskii, M.I.; Sumarokov, V.V.; Dolbin, A.V.; Nesov, S.N.; Korusenko, P.M.; Ponomarev, A.N.; et al. Calorimetric, NEXAFS and XPS Studies of MWCNTs with Low Defectiveness. *Fuller. Nanotub. Carbon Nanostruct.* **2021**, *29*, 331–336. [\[CrossRef\]](#)
- Zdanovich, A.A.; Moseenkov, S.I.; Ishchenko, A.V.; Kuznetsov, V.L.; Matsko, M.A.; Zakharov, V.A. The Morphology Evolution of Polyethylene Produced in the Presence of a Ziegler-type Catalyst Anchored on the Surface of Multi-Walled Carbon Nanotubes. *J. Appl. Polym. Sci.* **2021**, *138*, 50528. [\[CrossRef\]](#)
- Marek, E.J.; García-Calvo Conde, E. Effect of catalyst preparation and storage on chemical looping epoxidation of ethylene. *Chem. Eng. J.* **2021**, *417*, 127981. [\[CrossRef\]](#)
- Sanchez, N.; Ruiz, R.; Hacker, V.; Cobo, M. Impact of bioethanol impurities on steam reforming for hydrogen production: A review. *Int. J. Hydrog. Energy* **2020**, *45*, 11923–11942. [\[CrossRef\]](#)
- Skiba, E.A.; Ovchinnikova, E.V.; Budaeva, V.V.; Banzaraksaeva, S.P.; Kovgan, M.A.; Chumachenko, V.A.; Kortusov, A.N.; Mironova, G.F.; Parmon, V.N.; Sakovich, G.V. Miscanthus bioprocessing using HNO₃-pretreatment to improve productivity and quality of bioethanol and downstream ethylene. *Ind. Crop. Prod.* **2022**, *177*, 114448. [\[CrossRef\]](#)
- Skiba, E.A.; Baibakova, O.V.; Budaeva, V.V.; Pavlov, I.N.; Vasilishin, M.S.; Makarova, E.I.; Sakovich, G.V.; Ovchinnikova, E.V.; Banzaraksaeva, S.P.; Vernikovskaya, N.V.; et al. Pilot Technology of Ethanol Production from Oat Hulls for Subsequent Conversion to Ethylene. *Chem. Eng. J.* **2017**, *391*, 178–186. [\[CrossRef\]](#)
- Ovchinnikova, E.V.; Mironova, G.F.; Banzaraksaeva, S.P.; Skiba, E.A.; Budaeva, V.V.; Kovgan, M.A.; Chumachenko, V.A. Bioprocessing of Oat Hulls to Ethylene: Impact of Dilute HNO₃- or NaOH-pretreatment on Process Efficiency and Sustainability. *ACS Sustain. Chem. Eng.* **2021**, *9*, 16588–16596. [\[CrossRef\]](#)
- Banzaraksaeva, S.P.; Surmina, M.A.; Chumachenko, V.A.; Ovchinnikova, E.V. Effect of the Isopropanol Impurity in the Feed on Catalytic Dehydration of Bioethanol to Ethylene. *Russ. J. Appl. Chem.* **2020**, *93*, 721–728. [\[CrossRef\]](#)
- Le Valant, A.; Garron, A.; Bion, N.; Duprez, D.; Epron, F. Effect of higher alcohols on the performances of a 1%Rh/MgAl₂O₄/Al₂O₃ catalyst for hydrogen production by crude bioethanol steam reforming. *Int. J. Hydrog. Energy* **2011**, *36*, 311–318. [\[CrossRef\]](#)
- Bilal, M.; Jackson, S.D. Ethanol steam reforming over Pt/Al₂O₃ and Rh/Al₂O₃ catalysts: The effect of impurities on selectivity and catalyst deactivation. *Appl. Catal. A Gen.* **2017**, *529*, 98–107. [\[CrossRef\]](#)
- Sanchez, N.; Ruiz, R.Y.; Cifuentes, B.; Cobo, M. Controlling sugarcane press-mud fermentation to increase bioethanol steam reforming for hydrogen production. *Waste Manag.* **2019**, *98*, 1–13. [\[CrossRef\]](#)
- Le Valant, A.; Garron, A.; Bion, N.; Epron, F.; Duprez, D. Hydrogen production from raw bioethanol over Rh/MgAl₂O₄ catalyst impact of impurities: Heavy alcohol, aldehyde, ester, acid and amine. *Catal. Today* **2008**, *138*, 169–174. [\[CrossRef\]](#)
- Mohsenzadeh, A.; Zamani, A.; Taherzadeh, M.J. Bioethylene production from ethanol: A review and techno-economical evaluation. *ChemBioEng Rev.* **2017**, *4*, 75–91. [\[CrossRef\]](#)
- Banzaraksaeva, S.P.; Ovchinnikova, E.V.; Danilova, I.G.; Danilevich, V.V.; Chumachenko, V.A. Ethanol-to-Ethylene Dehydration on Acid-Modified Ring-Shaped Alumina Catalyst in a Tubular Reactor. *Chem. Eng. J.* **2019**, *374*, 605–618. [\[CrossRef\]](#)
- Yoo, K.-Y. Effects of Reactor Type on the Economy of the Ethanol Dehydration Process: Multitubular vs. Adiabatic Reactors. *Korean Chem. Eng. Res.* **2021**, *59*, 467–479. [\[CrossRef\]](#)
- Becerra, J.; Quiroga, E.; Tello, E.; Figueredo, M.; Cobo, M. Kinetic modeling of polymer-grade ethylene production by diluted ethanol dehydration over H-ZSM-5 for industrial design. *J. Environ. Chem. Eng.* **2018**, *6*, 6165–6174. [\[CrossRef\]](#)

24. Frosi, M.; Tripodi, A.; Conte, F.; Ramis, G.; Mahinpey, N.; Rossetti, I. Ethylene from renewable ethanol: Process optimization and economic feasibility assessment. *J. Ind. Eng. Chem.* **2021**, *104*, 272–285. [[CrossRef](#)]
25. Kagyrmanova, A.P.; Chumachenko, V.A.; Korotkikh, V.N.; Kashkin, V.N.; Noskov, A.S. Catalytic dehydration of bioethanol to ethylene: Pilot-scale studies and process simulation. *Chem. Eng. J.* **2011**, *176–177*, 188–194. [[CrossRef](#)]
26. Van der Borgh, K.; Alexopoulos, K.; Toch, K.; Thybaut, J.W.; Marin, G.B.; Galvita, V.V. First-Principles-Based Simulation of an Industrial Ethanol Dehydration Reactor. *Catalysts* **2019**, *9*, 921. [[CrossRef](#)]
27. Ovchinnikova, E.V.; Banzaraksheva, S.P.; Chumachenko, V.A. Optimal Design of Ring-Shaped Alumina Catalyst: A Way to Intensify Bioethanol-to-Ethylene Production in Multi-Tubular Reactor. *Chem. Eng. Res. Des.* **2019**, *145*, 1–11. [[CrossRef](#)]
28. Tripodi, A.; Belotti, M.; Rossetti, I. Bioethylene Production: From Reaction Kinetics to Plant Design. *ACS Sustain. Chem. Eng.* **2019**, *7*, 13333–13350. [[CrossRef](#)]
29. Maia, J.G.S.S.; Demuner, R.B.; Secchi, A.R.; Melo, P.A.; do Carmo, R.W.; Gusmão, G.S. Process Modeling and Simulation of an Industrial-Scale Plant for Green Ethylene Production. *Ind. Eng. Chem. Res.* **2018**, *57*, 6401–6416. [[CrossRef](#)]
30. Diaz de Leona, J.N.; Cruz-Taboada, A.; Esqueda-Barron, Y.; Alonso-Nuñez, G.; Loera-Serna, S.; Venezia, A.M.; Poisot, M.E.; Fuentes-Moyado, S. Catalytic dehydration of 2 propanol over Al₂O₃-Ga₂O₃ and Pd/Al₂O₃-Ga₂O₃ Catalysts. *Catal. Today* **2020**, *356*, 339–348. [[CrossRef](#)]
31. Bedia, J.; Ruiz-Rosas, R.; Rodríguez-Mirasol, J.; Cordero, T. A kinetic study of 2-propanol dehydration on carbon acid catalysts. *J. Catal.* **2010**, *271*, 33–42. [[CrossRef](#)]
32. El-Sharkawy, E.A.; Mostafa, M.R.; Youssef, A.M. Changes in surface and catalytic dehydration activities of 2-propanol on AlPO-5 induced by silver impregnation. *Colloids Surf. A Physicochem. Eng. Asp.* **1999**, *157*, 211–218. [[CrossRef](#)]
33. Garbarino, G.; Vijayakumar, R.P.P.; Riani, P.; Finocchio, E.; Busca, G. Ethanol and diethyl ether catalytic conversion over commercial alumina and lanthanum-doped alumina: Reaction paths, catalyst structure and coking. *Appl. Catal. B* **2018**, *236*, 490–500. [[CrossRef](#)]
34. Kagyrmanova, A.P.; Zolotarskii, I.A.; Vernikovskaya, N.V.; Smirnov, E.I.; Kuzmin, V.A.; Chumakova, N.A. Modeling of steam reforming of natural gas with shaped catalyst. *Theor. Found. Chem. Eng.* **2006**, *40*, 155–167. [[CrossRef](#)]
35. Kagyrmanova, A.P.; Zolotarskii, I.A.; Smirnov, E.I.; Vernikovskaya, N.V. Optimum Dimensions of Shaped Steam Reforming Catalysts. *Chem. Eng. J.* **2007**, *134*, 228–234. [[CrossRef](#)]
36. Smirnov, E.I.; Muzykantov, A.V.; Kuzmin, V.A.; Kronberg, A.E.; Zolotarskii, I.A. Radial heat transfer in packed beds of spheres, cylinders and Rashig rings Verification of model with a linear variation of λ_{er} in the vicinity of the wall. *Chem. Eng. J.* **2003**, *91*, 243–248. [[CrossRef](#)]
37. Zolotarskii, I.A.; Voennov, L.I.; Zudilina, L.Y.; Isupova, L.A.; Zotov, R.A.; Medvedev, D.A.; Stepanov, D.A.; Livanova, A.V.; Meshcheryakov, E.P.; Kurzina, I.A. Theoretical Optimization of the Shape and Size of Adsorbent Grains for Associated Petroleum Gas Drying. *Catal. Ind.* **2018**, *10*, 49–56. [[CrossRef](#)]
38. Ovchinnikova, E.V.; Vernikovskaya, N.V.; Andrushkevich, T.V.; Chumachenko, V.A. Mathematical modeling of β -picoline oxidation to nicotinic acid in multitubular reactor: Effect of the gas recycle. *Chem. Eng. J.* **2011**, *176–177*, 114–123. [[CrossRef](#)]
39. Ovchinnikova, E.V.; Chumachenko, V.A.; Valuiskikh, N.N. Influence of the process parameters on temperature conditions and productivity of multitubular reactor for methanol to formaldehyde oxidation. *Catal. Ind.* **2013**, *5*, 297–311. [[CrossRef](#)]
40. Ovchinnikova, E.V.; Chumachenko, V.A. Nicotinic acid synthesis at elevated β -picoline load: Exploring the possibility to intensify the process. *Chem. Eng. Res. Des.* **2021**, *171*, 63–72. [[CrossRef](#)]
41. Frank-Kamenetskii, D.A. Diffuziya i teploperedacha v khimicheskoi kinetike. In *Diffusion and Heat Transfer in Chemical Kinetics*; Nauka: Moscow, Russia, 1987.

Disclaimer/Publisher's Note: The statements, opinions and data contained in all publications are solely those of the individual author(s) and contributor(s) and not of MDPI and/or the editor(s). MDPI and/or the editor(s) disclaim responsibility for any injury to people or property resulting from any ideas, methods, instructions or products referred to in the content.